Contents

List of Figures

CHAPTER 4

Investigating the cause of the $\alpha - z$ relation

"Trying to predict the future is a mug's game. But increasingly it's a game we all have to play because the world is changing so fast and we need to have some sort of idea of what the future's actually going to be like because we are going to have to live there, probably next week."
−Douglas Adams−

Leah K. Morabito, Jeremy Harwood

The correlation between radio spectral index and redshift has long been used to identify high redshift radio galaxies, but its cause is unknown. Traditional explanations invoke intrinsic relations between spectral index and power, environmental differences at high redshift, or higher inverse Compton losses due to the increased photon energy density of the cosmic microwave background. In this paper we investigate whether the increased inverse Compton losses can cause the observed spectral index – redshift correlation by using spectral modelling of nearby radio galaxies to simulate their high redshift equivalents.

Morabito, L. K. and Harwood, J.
In preparation

4.1 Introduction

High redshift radio galaxies (HzRGs) are unique laboratories for studying the formation and evolution of massive galaxies, rich clusters and massive black holes at $z > 2$. They have extended jets on kpc scales that emit synchrotron radiation detectable in the radio regime. The host galaxies have clumpy optical morphologies (Pentericci et al., 2000) and optical spectra indicative of extreme star formation and large stellar masses. They are often found in protocluster environments (Pentericci et al., 2000) and are thought to evolve into present-day dominant cluster galaxies (Miley & De Breuck, 2008; Best et al., 1997). Less than 200 HzRGs are presently known (Miley & De Breuck, 2008), and the highest redshift radio galaxy to date is at $z = 5.19$ (van Breugel et al., 1999).

Almost all of these HzRGs were found by searches for ultra steep spectrum (USS; defined as $\alpha < -1$ where flux density is $S \propto \nu^{\alpha}$) sources in radio surveys. Tielens et al. (1979) first recognized that USS sources were three times less likely to have an optically identified host galaxy, and that their smaller angular sizes implied they were at larger distances. Blumenthal & Miley (1979) found that spectral index did indeed correlate with redshift, with steeper spectral indices associated with objects at higher redshift. Since then, searching for USS sources has been an effective way to identify candidate high redshift sources (e.g., Röttgering et al., 1994) that can be followed up with spectroscopic confirmation.

While the $\alpha - z$ correlation is useful for identifying high redshift galaxies, it is not understood what causes the relation. The traditional explanation is that the observed USS is due to a radio k-correction coupled with the fact that fixed observing frequencies probe higher rest frame frequencies of the radio spectra for higher redshift sources, where steepening due to synchrotron losses is more pronounced. The high-frequency spectra will also be impacted by losses due to inverse Compton scattering of cosmic microwave background (CMB) photons (Krolik & Chen, 1991). Klamer et al. (2006) investigated the rest-frame radio spectra of 37 USS HzRGs with matched-resolution observations spanning $2.3 - 6.2$ GHz and found that the k-correction did not impact the overall relation between spectral index and redshift.

Two alternative explanations have been proposed. The first is that higher ambient density could cause steeper electron energy spectra in the particle acceleration processes at the jet working surfaces. Higher ambient density is expected at higher redshifts, and the radio spectra of HzRGs could therefore be steeper than local radio galaxies (Athreya & Kapahi, 1998; Klamer et al., 2006). The attraction of this explanation is that it could result in both a $\alpha - z$ relation

and a $\alpha-$luminosity relation.

Another explanation is that the $\alpha - z$ relation arises naturally from a correlation between α and luminosity (Chambers et al., 1990; Blundell et al., 1999). For models where higher jet powers produce steeper integrated spectra, when taking Malmquist bias into account no intrinsic relation between $\alpha - z$ is necessary to match observations. It is difficult to study these kinds of effects observationally with flux density limited surveys. Ker et al. (2012) examined the essential relationships amongst power, linear size, redshift, and spectral index for both low and high frequency selected surveys separately, finding only a weak $\alpha - z$ relation which is dominated by the scatter in α. Their findings are consistent with the increasing ambient density at higher redshifts driving the $\alpha - z$ relation.

In this paper we focus on understanding both the cause and the individual selection effects that can impact the $\alpha - z$ relation with a new approach. Using the Broadband Radio Astronomy ToolS software package (BRATS[1]; Harwood et al., 2013, 2015), we fit integrated spectral ageing models to archival radio measurements to produce model radio spectra between 100MHz and 10 GHz. Assuming that HzRGs are similar to their local counterparts (supported by the findings in Morabito et al., 2016), we construct a sample which has no initial dependence between α and z and simulate the sources at higher redshifts to introduce inverse Compton losses and selection effects individually. By doing so we can determine if the observed $\alpha - z$ relation can be reproduced via these effects alone.

In Section 4.2 we describe the initial sample. In Section 4.3 we explain how we use BRATS to model the data, and the introduction of selection effects. Results are presented in Section 4.4 followed by discussion and conclusions in Section 4.5. Throughout the paper we assume a ΛCDM concordance cosmology with $H_0 = 67.8\ \mathrm{km\,s^{-1}\,Mpc^{-1}}$, $\Omega_\mathrm{m} = 0.308$, and $\Omega_\Lambda = 0.692$, consistent with Planck Collaboration et al. (2015).

4.2 Initial Sample

4.2.1 Archival Radio Spectral Energy Distributions

Integrated flux density measurements are required across a wide range of frequencies to perform robust spectral modelling. It is important to capture the behaviour of the radio spectral energy distribution (SED) both at low and high frequencies, in order to fit for any curvature in the overall SED. In practice, this

[1] http://www.askanastronomer.co.uk/brats

generally means a minimum of two flux density measurements at frequencies less than ∼ 500 MHz and three measurements above ∼ 500 MHz. Extremely low frequencies ($\lesssim$ 100 MHz) can be impacted by free-free absorption and/or synchrotron self-Compton absorption, and will not be well-fitted by spectral ageing models that do not include these physical processes. At frequencies higher than ∼ 10 GHz, most sources will be highly resolved and integrated flux density measurements will be unreliable. We therefore construct SEDs over frequencies from ∼ 100 MHz to 10 GHz.

We started by searching the NASA/IPAC Extragalactic Database[2] for all objects with $z \leq 1$ and having radio photometry available at 178 MHz. This is the frequency of the 3CRR survey (Laing et al., 1983), which is a 96 per cent complete spectroscopic survey containing the type of bright, jetted radio sources we are interested in. This provided 840 sources, 777 of which had spectroscopic redshifts. We used the new TIFR GMRT Sky Survey Alternative Data Release 1 (TGSS ADR1; Intema et al., 2016) to provide an additional low-frequency measurement at 150 MHz and we cross-matched the 777 NED objects with the TGSS catalogue. There were 259 objects matched within a search radius of 12.5 arcsec (half the size of the average beam size in TGSS).

From the NED flux density measurements we automatically removed individual measurements that were marked as 'peak', 'core', or 'lobe' values. Measurements within 5 MHz of each other were averaged together and their errors added in quadrature. We required that each spectrum have at least two measurements below 500 MHz and three measurements above 500 MHz. There were 155 sources that met this criteria. We visually inspected the SEDs to identify and remove individual aberrant flux density measurements. We also removed 12 flat-spectrum sources, 1 Gigahertz-peaked source, and 5 nearby star-forming galaxies. This left us with a total of 137 sources.

We used BRATS to fit all radio spectra with a continuous injection model (Pacholczyk, 1970) for a range of initial electron energy distributions (injection index), from $\alpha_{inj} = 0.5$ to 1.0 in steps of 0.05. We assume a fixed magnetic field of 1×10^{-9} nT. While there is almost certainly a range of magnetic field strengths within our sample, the radiative losses (hence observed spectral index) are proportional to both the magnetic field strength of the source and the equivalent field of the CMB where $B = \sqrt{B_{lobe}^2 + B_{CMB}^2}$. Due to the equivalent field strength scaling as a function of redshift such that $B_{CMB} = 0.318(1+z)^2$,

[2]The NASA/IPAC Extragalactic Database (NED) is operated by the Jet Propulsion Laboratory, California Institute of Technology, under contract with the National Aeronautics and Space Administration.

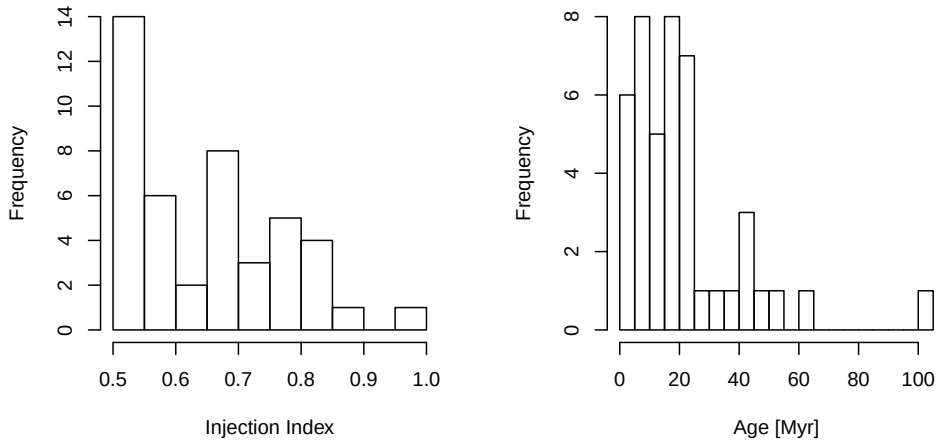

Figure 4.1: Distributions of initial spectral modelling parameters.

it is this term which dominates at high redshifts. It is these sources which most strongly influence the $\alpha - z$ relation and so the effect of any variations in our initial sample should not impact significantly on our overall result.

The output of this spectral modelling includes the spectral age, CMB magnetic field energy density, break frequency in the spectrum, χ^2 of the fit, and confidence level of the fit. Taking only the fits with confidence levels of 1σ, we use the χ^2 values to select the best injection index for each source. We removed two sources because the spectral modelling produced ages consistent with zero. We also removed three sources which were not well-fit due to low-frequency turnovers in their spectra. This left a total of 42 sources in the initial sample, and we show the distributions of parameters associated with the fits in Fig. 4.1.

BRATS also outputs rest frame model spectra, and we use these to measure the $\alpha - z$ relation for our initial sample, which contained only the radio galaxies with $z \leq 1$. De Breuck et al. (2000) calculated α using fixed observing frequencies of 325 or 365 MHz for the low-frequency point, and 1.4 GHz for the high frequency point. Here we use fixed observing frequencies of 325 MHz and 1.4 GHz to calculate α. Fig. 4.2 shows the $\alpha - z$ relation for the initial sample, using the rest-frame model spectra. A linear fit to the data shows the slope is 0.033 ± 0.071, which is consistent with zero.

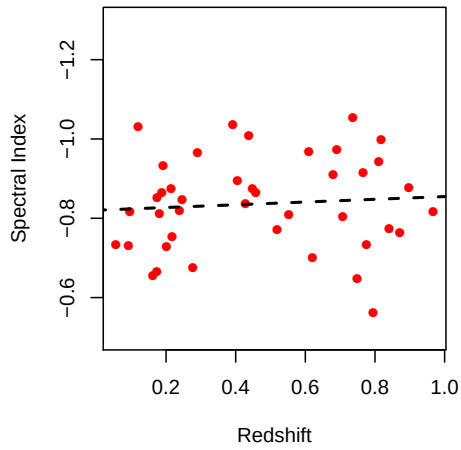

Figure 4.2: The $\alpha - z$ relation for the initial sample, which is limited to $0.1 \leq z \leq 1$. A linear fit to the data (red line) shows a slope of 0.033 ± 0.071, which is consistent with zero.

4.2.2 Constructing a High-redshift Sample

We construct a high-redshift sample by using the observed distribution of redshifts from De Breuck et al. (2000). We fit a power-law to the observed redshift distribution and use the acceptance-rejection method to simulate 10^6 redshifts consistent with this distribution (Fig. 4.3). Drawing from the simulated redshift distribution, we assign redshifts randomly to sources in our initial sample, taking care to match the observed redshift distribution. Some of the sources from our initial sample are used more than once, to match the total number of sources in the observed sample.

4.3 Modelling the Selection Effects

4.3.1 *k*-correction

The first selection effect we model is the *k*-correction. For this, we simply take the high-redshift sample and *k*-correct the rest-frame spectra to the observed frame using the simulated redshifts. We then measure the observed model spectra at fixed frequencies of 325 MHz and 1.4 GHz, and perform a linear fit to measure the slope of the relation between α and z. The redshift distribution and observed α-z relation are shown in Fig. 4.3. The linear fit to the data shows the slope of the relation is now 0.041 ± 0.010, which is slightly steeper but still consistent with the initial sample (within the uncertainties).

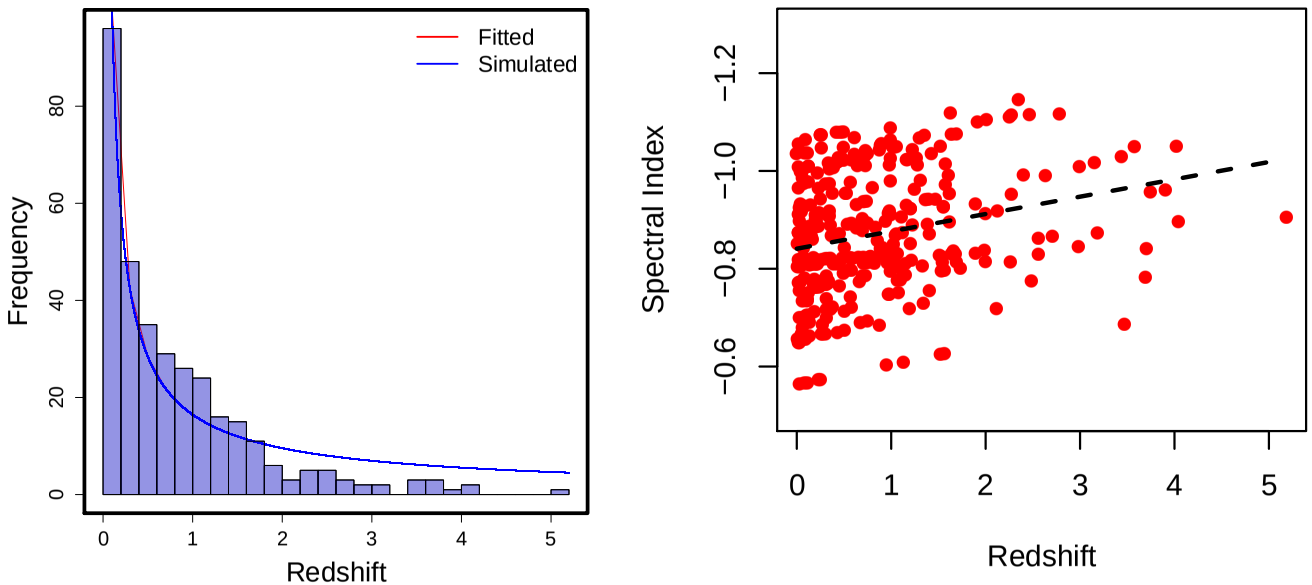

Figure 4.3: *Left:* The redshift distribution from De Breuck et al. (2000). The red line is a fit to the redshift distribution, and the blue line shows our simulated redshifts. The redshifts for the simulated sample are drawn from the simulated distribution, taking care to match the redshift distribution in the De Breuck et al. (2000) sample. *Right:* The sample of local galaxies that have been k-corrected with their simulated higher redshifts, drawn from the redshift distribution on the left.

4.3.2 Inverse Compton from CMB

To model the inverse Compton scattering from CMB photons, we take the rest-frame high redshift spectra and fix the ages and injection index from the initial BRATS models. We again perform spectral fitting using BRATS, but this time using the simulated redshifts, which introduces the $B_{\rm iC}$ term due to the inverse Compton scattering from the CMB. Fixing the ages insures that the only difference in the resultant model spectra is the effects of inverse Compton scattering. We again k-correct the rest-frame model spectra to the observed frame and measure the spectral index between 325 MHz and 1.4 GHz.

4.3.3 Observational Biases

To compare with the sample from De Breuck et al. (2000) we must be careful to use only objects from the simulated sample that would satisfy the selection effects in the observed sample. The 3CR and MRC samples are complete down to their flux density limits, but De Breuck et al. (2000) use other samples of USS sources selected from larger, incomplete samples. We therefore select objects to be included in the 'observed' simulated sample if they satisfy either of the following criteria:

- The source is above the flux density limit of the 3CR sample (10 Jy) with a redshift $\leq z_{max}$ of the 3CR sample ($z_{max} = 2.474$).
- The source is above the flux density limit of the 4C sample (2 Jy) with a spectral index at least as steep as $\alpha = -1.03$, the limiting spectral index for this sample in De Breuck et al. (2000).

4.4 Results

We plot the final results in Fig. 4.4. Shown in the figure are the observed sample from De Breuck et al. (2000), the entire high-redshift sample with inverse Compton effects modelled in the spectra, and the sample which also matches the selection criteria described in the last section. The linear fits of the simulated sample matching the selection criteria and the observed sample are also shown. We find $\alpha = -(0.16 \pm 0.0090)z - 0.79 \pm 0.0096$ for the simulated sample including selection effects and $\alpha = -(0.16 \pm 0.018)z - 0.75 \pm 0.021$ for the observed sample. These relations are consistent with each other within the uncertainties, and we find that the inverse Compton scattering from the CMB photons can entirely explain the $\alpha - z$ relation without invoking any environmental or intrinsic differences at high redshift.

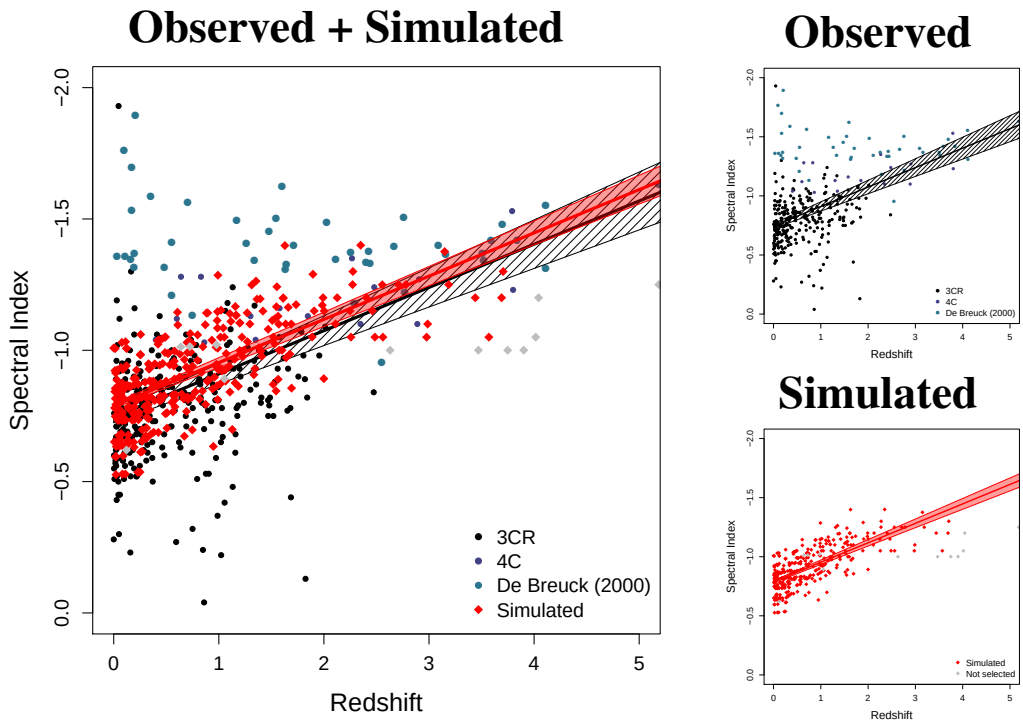

Figure 4.4: The $\alpha - z$ for the observed and simulated samples. The large panel on the left shows both observed and simulated samples together, while the panels on the right show the observed (*top*) and simulated (*bottom*) samples separately. The black points are from the 3CR survey, the dark blue points are from the 4C survey, and the points are the new additions of De Breuck et al. (2000). A linear fit to the observed sample is shown by the black line, with the hatched area representing the fit errors. The simulated data which meet the selection criteria explained in Section 4.3 are plotted as red diamonds, with a linear fit shown by a red line with the corresponding uncertainties in the shaded red area. Gray points are the simulated data that did not meet the selection criteria.

The scatter of measured spectral indices in the simulated sample is smaller than that in the observed sample, as evident in Fig. 4.4, but the fitted relations still agree at low redshift. At $z \leq 2$ this is partially due to our assumption of a single magnetic field strength, but also note that the USS objects at low redshift come from a positive bias, i.e., searches for USS objects in large, incomplete surveys. The scatter in our simulated sample is more comparable to the scatter in the 3CR survey, which is complete.

4.5 Discussion and Conclusions

In this paper we have used spectral modelling of a sample of local bright radio sources to simulate HzRGs and show that the observed $\alpha - z$ relation can be entirely reproduced by a combination of inverse Compton scattering from the CMB and selection effects. One final selection effect to consider in this analysis is that the sizes of radio galaxies decrease with increasing redshift (e.g., Morabito et al. 2016, Neeser et al., 1995). There is also a dependence of integrated spectral index on size, which Ker et al. (2012) have quantified as $\alpha = -0.07\mathrm{D} - 0.94$. Assuming the evolutionary dependence is $D \propto (1+z)^{-n}$ with $n = 1.99^{+0.25}_{-0.27}$ (Morabito et al., in preparation), the spectral index would tend to flatten towards higher redshift, but only by $\Delta\alpha \lesssim 0.1$ at $z = 5$. This is consistent with the differences we see in the simulated and observed samples.

We conclude that the $\alpha - z$ relation can be explained entirely by the enhanced inverse Compton losses at higher redshift, coupled with selection effects that are biased towards selecting USS sources from incomplete surveys. The $\alpha - z$ relation is still useful for finding candidate high-redshift galaxies, but we note that perhaps more high redshift sources could be found by relaxing the strict USS criteria to $\alpha < -0.9$ or < -0.8, and coupling the selection with size as suggested by Ker et al. (2012).

Acknowledgements

LKM acknowledges financial support from NWO Top LOFAR project, project n. 614.001.006.

Bibliography

Athreya R. M., Kapahi V. K., 1998, Journal of Astrophysics and Astronomy, 19, 63

Best P. N., Longair M. S., R"ottgering H. J. A., 1997, ArXiv Astrophysics e-prints,

Blumenthal G., Miley G., 1979, A&A, 80, 13

Blundell K. M., Rawlings S., Willott C. J., 1999, AJ, 117, 677

Chambers K. C., Miley G. K., van Breugel W. J. M., 1990, ApJ, 363, 21

De Breuck C., van Breugel W., Röttgering H. J. A., Miley G., 2000, AAPS, 143, 303

Harwood J. J., Hardcastle M. J., Croston J. H., Goodger J. L., 2013, MNRAS, 435, 3353

Harwood J. J., Hardcastle M. J., Croston J. H., 2015, MNRAS, 454, 3403

Intema H. T., Jagannathan P., Mooley K. P., Frail D. A., 2016, preprint, (arXiv:1603.04368)

Ker L. M., Best P. N., Rigby E. E., Röttgering H. J. A., Gendre M. A., 2012, MNRAS, 420, 2644

Klamer I. J., Ekers R. D., Bryant J. J., Hunstead R. W., Sadler E. M., De Breuck C., 2006, MNRAS, 371, 852

Krolik J. H., Chen W., 1991, AJ, 102, 1659

Laing R. A., Riley J. M., Longair M. S., 1983, MNRAS, 204, 151

Miley G., De Breuck C., 2008, A&ARv, 15, 67

Morabito L. K., et al., 2016, MNRAS, 461, 2676

Neeser M. J., Eales S. A., Law-Green J. D., Leahy J. P., Rawlings S., 1995, ApJ, 451, 76

Pacholczyk A. G., 1970, Radio astrophysics. Nonthermal processes in galactic and extragalactic sources

Pentericci L., et al., 2000, A&A, 361, L25

Planck Collaboration et al., 2015, preprint, (arXiv:1502.01589)

Röttgering H. J. A., Lacy M., Miley G. K., Chambers K. C., Saunders R., 1994, AAPS, 108

Tielens A. G. G. M., Miley G. K., Willis A. G., 1979, AAPS, 35, 153

van Breugel W., De Breuck C., Stanford S. A., Stern D., Röttgering H., Miley G., 1999, ApJL, 518, L61